Optical properties of passivated Si nanocrystals and SiO_x nanostructures

L. N. Dinh
Department of Applied Science, University of California, Davis/Livermore, California and Chemistry and Materials Science Department, University of California, Lawrence Livermore National Laboratory, Livermore, California 94550

L. L. Chase, M. Balooch, and W. J. Siekhaus
Chemistry and Materials Science Department, University of California, Lawrence Livermore National Laboratory, Livermore, California 94550

F. Wooten
Department of Applied Science, University of California, Davis/Livermore, California 94550
(Received 20 February 1996)

Thin films of Si nanoclusters passivated with oxygen or hydrogen, with an average size of a few nanometers, have been synthesized by thermal vaporization of Si in an Ar buffer gas, followed by subsequent exposure to oxygen or atomic hydrogen. High-resolution transmission electron microscopy and x-ray diffraction revealed that these nanoclusters were crystalline. However, during synthesis, if oxygen was the buffer gas, a network of amorphous Si oxide nanostructures (an-SiO_x) with occasional embedded Si dots was formed. All samples showed strong infrared and/or visible photoluminescence (PL) with varying decay times from nanoseconds to microseconds depending on synthesis conditions. Absorption in the Si cores for surface passivated Si nanocrystals (nc-Si), but mainly in oxygen related defect centers for an-SiO_x, was observed by photoluminescence excitation spectroscopy. The visible components of PL spectra were noted to blueshift and broaden as the size of the nc-Si was reduced. There were differences in PL spectra for hydrogen and oxygen passivated nc-Si. Many common PL properties between oxygen passivated nc-Si and an-SiO_x were observed. Our data can be explained by a model involving absorption between quantum confined states in the Si cores and emission for which the decay times are very sensitive to surface and/or interface states. The emission could involve a simple band-to-band recombination mechanism within the Si cores. The combined evidence of all of our experimental results suggests, however, that emission between surface or interface states is a more likely mechanism. [S0163-1829(96)08731-0]

I. INTRODUCTION

The use of Si in optical applications is limited by its small and indirect band gap. However, recent observations of visible photoluminescence (PL) in porous Si (Ref. 1) and Si ultrafine particles[2–4] suggest that Si nanoclusters may become a promising material for optical applications, if their electronic and optical properties were well understood. As of now, the mechanism of the observed visible PL is still under debate.[5–19] Some researchers attribute the PL to quantum confinement effects in the Si nanostructures,[1,8,13] while others attribute it to amorphous Si,[14,15] siloxene,[10,16] hydrides/polysilanes,[17,18] and oxygen-related defect centers.[3,7,19] Consensus is difficult to reach, especially in the case of porous Si because of the coexistence of a large variety of surface chemistries and structures in this system. In order to shed more light on this matter, it seems useful to first examine more controllable systems, such as silicon nanocrystals (nc-Si), with well controlled surface chemistry and sizes, and silicon oxide nanostructures (an-SiO_x), whose luminescence properties have some similarities to porous silicon. In this paper, we show how nc-Si will small size distribution and an-Si-O_x can be synthesized in a well-controlled environment. The effects of surface passivation of nc-Si of different sizes with hydrogen or oxygen at different temperatures on the observed PL are presented. Photoluminescence excitation (PLE) spectra and PL decay times of nc-Si and an-SiO_x are reported. A comparison of the many different and common PL properties among the passivated nc-Si and an-SiO_x is included. Finally, we will also discuss how this comparison leads us to attribute the mechanism of the observed PL from nc-Si to a model involving absorption mainly in the Si cores, and emission due to transition between defect states in the passivation layer.[6,9,11,12]

II. EXPERIMENTS

The synthesis chamber was an ultrahigh vacuum (UHV) chamber with a base pressure of $<5\times10^{-10}$ Torr. This chamber was equipped with a fused silica window for optical spectroscopies, a Nanoscope III scanning tunneling microscope (STM) from Digital Instruments, and a double pass cylindrical mirror analyzer for Auger electron spectroscopy (AES) and x-ray photoelectron spectroscopy (XPS).

For the synthesis of nc-Si, the technique of thermal vaporization of Si in a buffer gas[20,21] was employed. In this technique, the chamber was filled with Ar gas up to the desired pressure. Premelted and outgassed Si inside a carbon boat, which was fitted inside a W basket, was resistively heated up to a few hundred degrees above its melting point

(as measured by an optical pyrometer). The substrates used to collect nc-Si powders were highly oriented pyrolytic graphite (HOPG) surfaces, glass slides, fused silica, or sheets of Mo or Ta, and were mounted from 5 to 8 cm directly above the evaporation boat. A manually operated shutter was placed between the evaporation boat and the substrate holder to control the Si arrival fluences. The average size of the Si clusters synthesized by this technique could be varied by increasing (or decreasing) the Si source temperature, the Ar buffer gas pressure, the source to substrate distance, or a combination of all these parameters. To produce H passivated nc-Si, the Ar buffer gas was pumped out of the synthesis chamber after the deposition of roughly one layer of nc-Si (as observed by STM). The sample was then exposed to atomic hydrogen by passing molecular hydrogen at 2×10^{-6} Torr through a very fine tungsten mesh at 2000 °C. This is a well-known technique to passivate Si wafers with hydrogen.[22,23] After 5 min of exposure and a subsequent removal of hydrogen, Ar was reintroduced into the synthesis chamber. Then, roughly another layer of nc-Si was deposited, and the process was repeated until a thick film was formed. To produce oxygen passivated nc-Si, the procedure was similar to the case of hydrogen passivated nc-Si, except that molecular oxygen at 300 mTorr and room temperature was used instead of atomic hydrogen; and after the desired film thickness was reached, the sample was resistively annealed in 4×10^{-4} Torr of oxygen to some predetermined temperatures. To produce an-SiO_x, the synthesis chamber was filled up to several mTorr of O_2 prior to Si deposition.

Characterization of the size and morphology of the synthesized material was done *in situ* using STM and *ex situ* using high-resolution transmission electron microscopy (HRTEM) and x-ray diffraction (XRD). The HRTEM observations were performed using a JEOL JEM4000EX instrument, operating at 400 kV accelerating voltage, with 1.6-Å resolution. Samples were taken out of the synthesis chamber and prepared by gently scraping the Si film off its substrate surface using a blunt scalpel taking care not to scratch the substrate itself. The film was then collected onto an amorphous carbon-coated Cu HRTEM grid. XRD measurements using the Cu $K\alpha_1$ line were performed on Si films deposited on glass slides.

Photoluminescence (PL) measurements were performed in the UHV system. The excitation source was either a 15 mW, 325 nm, continuous wavelength He-Cd laser (Omnichrome, series 56) or a Spectra Physics Ar ion laser operating at 488.8 nm. PL spectra were measured with a grating spectrometer (Oriel Multispec) and an Oriel Instaspec IV cooled charged-coupled Si detector array. All PL spectra have been corrected for instrument response using a calibrated lamp traceable to NIST standards.

For measurements of PL decay times, an excimer laser (Questek, series 2000) operating at 308 nm with a pulse duration of 20 ns was used for excitation. A photomultiplier tube with GaAs photocathode, providing extended red response and a rise time of 12 ns, was used for detection at the output of the monochromator. Neutral density filters were employed so that the excimer laser beam, upon striking a sample surface of a few mm^2, had an energy of a few μJ.

For PLE measurements, white light from a 1-kW mercury-xenon arc lamp was passed through appropriate order selection filters and then focused onto the input slit of a monochromator. Monochromatic light from the output of the monochromator was then used to excite the luminescence from the sample. A broadband optical detector monitored the energy flux at the output of the monochromator, and this was used to normalize the PLE spectra for the variation of intensity as a function of excitation energy.

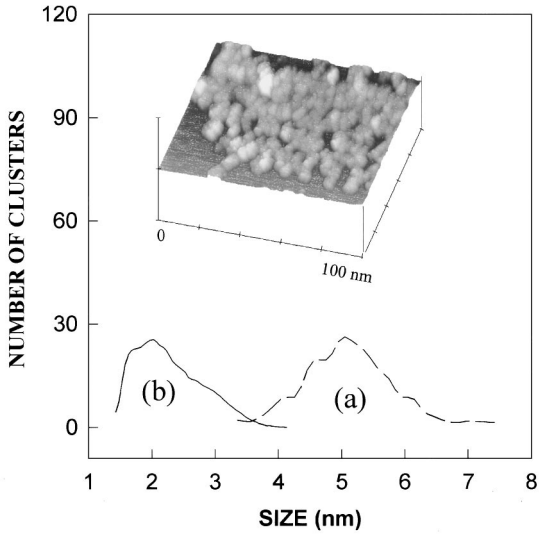

FIG. 1. Size distributions of the Si cores of a sample deposited on a HOPG substrate by vaporization of Si at 1700 °C in an Ar pressure of 500 mTorr, and a source-to-substrate distance of 5 cm (a) before oxygen passivation and (b) after oxygen passivation. The inset shows an STM image of roughly one layer of such Si clusters before oxygen passivation.

III. EXPERIMENTAL RESULTS

A. Surface passivated nc-Si

1. Size, composition, and crystallinity

The inset of Fig. 1 shows a constant current STM image of approximately 1 ML of Si clusters, with average diameters of 5 nm before oxidation, deposited on a HOPG substrate by vaporization of Si at 1700 °C in an Ar buffer gas of 500 mTorr, and at a source to substrate distance of 5.0 cm. Figure 1(a) shows the distribution of diameters determined by STM (Ref. 24) from a collection of 300 Si clusters of the same sample. The actual STM image is shown in the inset of Fig. 1. An average diameter of about 5 nm and a full width at half maximum (FWHM) of about 2 nm are observed. Figure 1(b) shows a distribution of diameters of the Si cores of 250 Si clusters from the same sample as in the inset obtained from HRTEM measurements after a surface oxide layer has formed during oxidation in dry oxygen up to 800 °C for 5 min. The sharp cutoff at small nanocluster size is an artifact due to the difficulty in reliably detecting, with our HTREM, clusters smaller than 1 nm in diameter. The average diameter of these cluster cores is approximately 2 nm, so the thickness of the silicon oxide layer on these nanocrystals is about 1.5 nm. Other samples with average cluster size in the range of 2–6.5 nm also have size distributions with FWHM of about 2.0 ± 0.2 nm, and silicon oxide outer layers with thickness of about 1.2–1.5 nm.

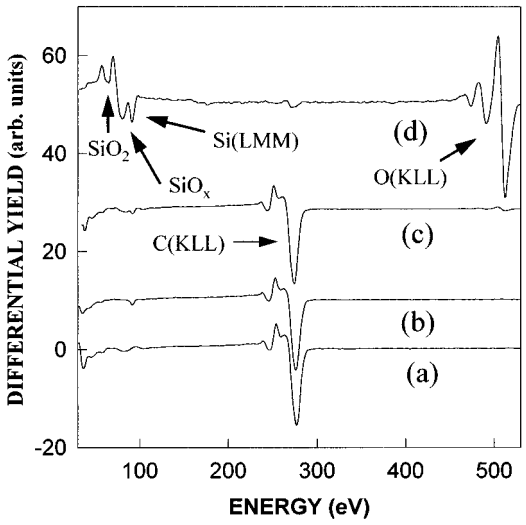

FIG. 2. (a) AES spectra of a clean HOPG surface, (b) with roughly one layer of Si nanocrystals before any oxygen exposure, (c) after exposure to 300 mTorr of oxygen at room temperature, and (d) after the formation of a thick film of oxygen passivated nanocrystals.

The composition of the as-deposited Si nanoclusters during synthesis was monitored by AES. In Fig. 2, curve (a) shows the AES spectrum from the degassed HOPG substrate. The dip around 272 eV is the C (KLL) Auger transition from the HOPG substrate. A small dip at about 92 eV due to the Si (LMM) Auger transition was observed after the deposition of roughly one layer of Si clusters [curve (b)]. Note that there was no observable oxygen contamination. But after 5 min of exposure to 300 mTorr of molecular oxygen, a small dip at about 503 eV due to the O (KLL) Auger transition was present [curve (c)]. The above process was continued one layer of clusters at a time until a thick film of surface oxidized Si nanoclusters was obtained [curve (d)]. The dips near 60 and 80 eV are signatures of SiO_2 and SiO_x $(0<x\leqslant 2)$, respectively.

HRTEM and XRD revealed that Si nanoclusters synthesized by our technique had the cubic crystalline structure of bulk silicon. Figure 3 shows an XRD plot of a sample of Si nanoclusters deposited on a glass slide by vaporization of Si at 1900 °C in an Ar pressure of 3000 mTorr, and at a source-to-substrate distance of 6.5 cm. This sample was a film of about 10 μm thick of initially unpassivated nanocrystals, and was exposed to air for 2 days prior to XRD measurement. In Fig. 3, the lower curve shows Si diffraction peaks from the (111), (220), and (311) planes of a calibration sample of microcrystalline Si powder with grain sizes >10 μm. All of the allowed diffraction peaks from the calibration sample were present in the sample of silicon nanocrystals. The diffraction peaks of the nanocrystalline film are broadened due to the small size of the crystals. From the Sherrer formula[25] and the width of the diffraction peaks, the average diameter of nc-Si was determined to be 8 nm for this sample. Strain and stress on these nc-Si could contribute to the observed broadening.[26] This effect was probably small, however, because there was reasonable agreement between the XRD and HRTEM measurements on similar samples. The inset of Fig. 3 shows an HRTEM image of a Si nanocrystallite from a

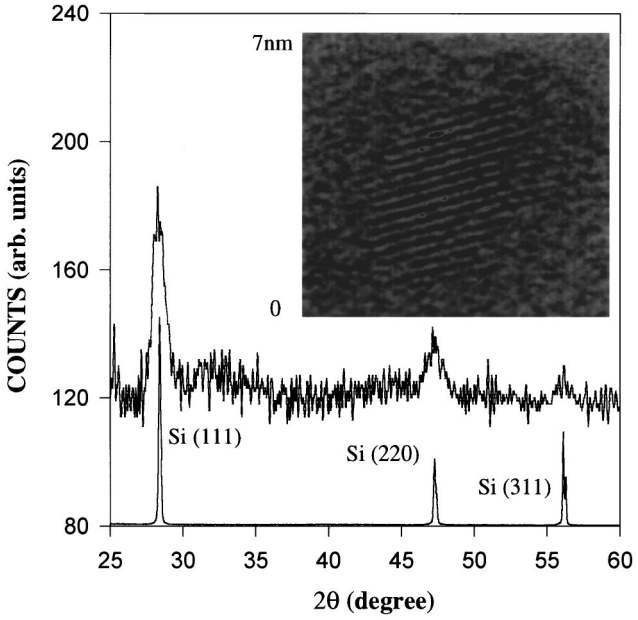

FIG. 3. XRD of large grain Si microcrystals (bottom curve), and of Si nanocrystals deposited on a glass slide by vaporization of Si at 1900 °C in an Ar pressure of 3000 mTorr, and a source-to-substrate distance of 6.5 cm (upper curve). The inset shows an HRTEM image of a Si nanocrystallite in an amorphous SiO_x matrix on an amorphous carbon-coated Cu HRTEM grid. This sample was synthesized by vaporization of Si at 1700 °C in an Ar pressure of 2000 mTorr, and a source-to-substrate distance of 5 cm.

sample deposited on a Mo substrate by vaporization of Si at 1700 °C, in an Ar pressure of 2000 mTorr, and at a source-to-substrate distance of 5 cm. This sample was not passivated, and was air exposed for 2 days prior to HRTEM measurement. As can bee seen in the inset, Si lattice fringes, from (111) planes with lattice spacing of about 0.3134 nm, were clearly observed in a background of amorphous Si oxide, on the amorphous carbon-coated Cu HRTEM grid. This particular Si nanocrystallite had a Si core of about 4.7 nm in diameter, which was also the average size for the film. It was also observed from HRTEM that the oxide layers covering the Si cores from all of our samples varied between 1.2 and 1.5 nm whether they were air exposed for 2 days or 2 weeks. This result was also true for samples subjected to annealing to 800 °C for 5 min in dry oxygen of about 4×10^{-4} Torr. So, in general, our synthesized Si clusters were nc-Si, the surfaces of which were either terminated with hydrogen, or, if passivated with oxygen, they were covered with 1.2–1.5-nm-thick layers of SiO_x $(0<x\leqslant 2)$.

2. PL properties

Unpassivated nc-Si did not exhibit any PL detectable by our Si detector in the energy range >1.2 eV, this is expected due to the quenching effect of the dangling bonds. However, all surfaces passivated nc-Si showed easily detectable infrared and/or visible PL, the intensity of which depended roughly linearly on the exciting laser beam intensity. It was also observed that excitation by either the 325-nm line from the He-Cd laser or the 488.8-nm line from the Ar ion laser produced similar PL shape for a given sample.

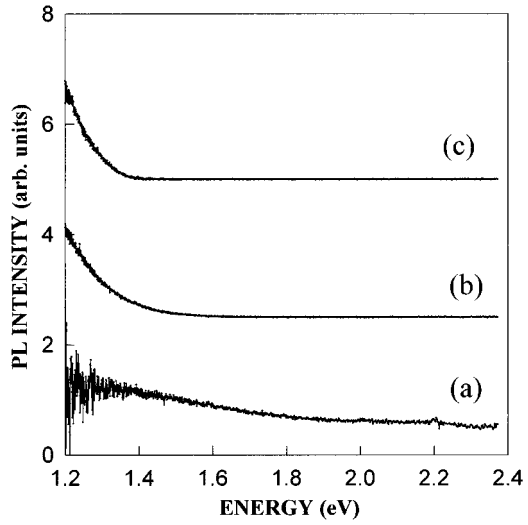

FIG. 4. PL spectra of hydrogen passivated nc-Si of average diameters of (a) 3.5 nm, (b) 5 nm, and (c) 6.5 nm.

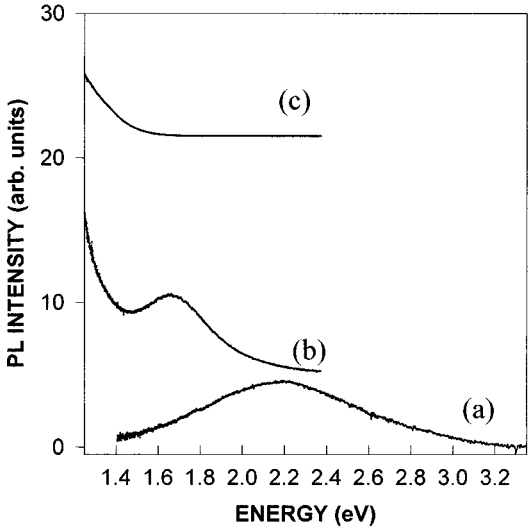

FIG. 5. PL spectra of oxygen passivated nc-Si with average Si core diameters, after annealing in dry oxygen up to 800 °C, of (a) 2.0 nm, (b) 3.5 nm, and (c) 4.7 nm.

Figure 4 shows PL spectra from hydrogen passivated nc-Si. Curves (a), (b), and (c) correspond to PL from samples made by vaporization of Si at 1700 °C, at a source-to-substrate distance of 5 cm, and in Ar pressures of 250, 500, and 1000 mTorr, respectively. STM measurements of average diameter of these nc-Si yielded average values of 3.5, 5.0, and 6.5 nm for curves (a), (b), and (c), respectively. All three samples exhibited strong near-infrared PL, accompanied by increasing PL intensity at energies below 1.2 eV. A comparison of the relative intensities among the three curves was not possible, since the three samples had different amounts of compactness and film thickness. With decreasing nanocrystal size, however, slight blueshifts were observed for PL edges on the higher-energy side of the PL spectra. The increasing PL intensity at photon energies below 1.2 eV is a distinctive characteristic of these hydrogen passivated nanocrystals. This behavior distinguishes them from porous silicon, which has luminescence peaks in the red to the near infrared, accompanied in some cases by additional luminescence peaks below 1.2 eV.[27,28] The increasing PL in our samples at photon energies below ~1.2 eV suggests that the surface passivation for our samples is not complete. Optical transitions between states lying in the nc-Si energy gaps are probably responsible for this PL.

Larger PL blueshifts with decreasing nanocrystal size were observed with oxygen passivated nc-Si. This is illustrated in Fig. 5; curves (a), (b), and (c) correspond to PL from samples made by vaporization of Si at 1700 °C onto HOPG substrates, at a source-to-substrate distance of 5 cm, and in an Ar pressure of 500, 1000, and 2000 mTorr, respectively. These samples were exposed to oxygen after each monolayer of nc-Si was deposited, and later annealed in steps of 150 °C for 5 min/step up to 800 °C. Sample (a) had an average nc-Si diameter of 5 nm before oxidation, and average unoxidized Si core diameter of 2 nm after oxidation. This sample exhibited a strong orange-white PL, with a PL peak at around 2.2 eV. Samples *b* had an average diameter of 6.5 nm before oxidation, and an average unoxidized Si core diameter after oxidation of 3.5 nm. This sample had a bright red PL, with a PL peak at about 1.7 eV and an increase in intensity at lower energies in the infrared. Sample (c) had an average unoxidized Si core diameter of 4.7 nm after oxidation, and exhibited a dark red PL, with PL increasing in the infrared. It is noted that the visible components of the PL spectra from these passivated nc-Si were very broad, and that as the nanocrystal size was reduced, PL broadening accompanied PL blueshift. The width of the observed PL could be explained by the distributions of sizes in our nc-Si, and therefore of energy gaps. For example, curve (a) in Fig. 5 has a PL with a FWHM of about 1 eV and a size distribution of about 2 nm, FWHM. This observed PL width is about 0.2–0.6 eV narrower than calculated bandwidths for interband transitions in Si nanocrystals.[29,30]

It is of interest to compare the energies of the observed emission bands with recent calculations of photon energies of interband recombination transitions in Si nanocrystals. The calculations of PL energy versus nc-Si diameter from Refs. 29 and 30 are shown in Fig. 6. In this figure, the dotted and continuous curves correspond to results from Refs. 29 and 30, respectively. The solid circles represent PL peak energies measured from samples of our oxygen passivated nc-Si. The error bars represent size distributions. The shaded area represents the region of PL intensity measured from our hydrogen passivated nc-Si, for which no emission peaks were observed above 1.2 eV. As can be observed, there are differences in our measured PL peak energies from oxygen and hydrogen passivated nc-Si. The PL peak energies from our oxygen passivated nc-Si are observed to stay closer to Ref. 30, while the ones from our hydrogen passivated nc-Si are below both reference curves. From Fig. 6, it is also clear that increased PL broadening due to dispersion of nanocrystal size is expected as the average size of nc-Si decreases, because quantum confinement effects are stronger in smaller nanocrystals. The comparison between our experimental energies and the calculations suggests that the emissions we observed could result from electron-hole recombination transitions in the Si cores. However, the observed PL energies

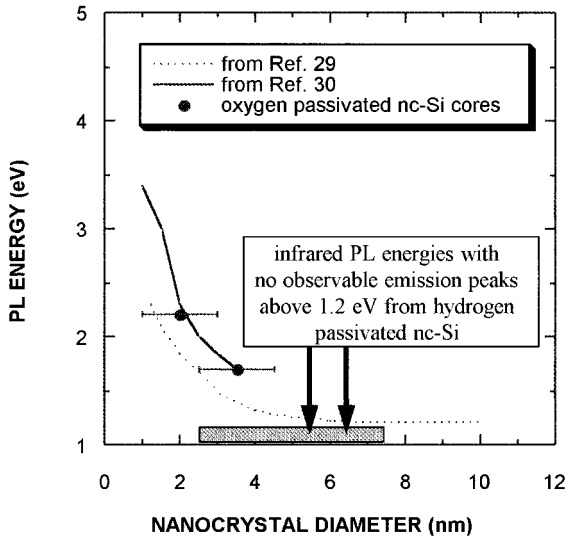

FIG. 6. Theoretical PL energy vs nanocrystal diameter for nc-Si from Refs. 29 and 30. Experimental values are from Figs. 4 and 5 of this work. Error bars represent size distributions.

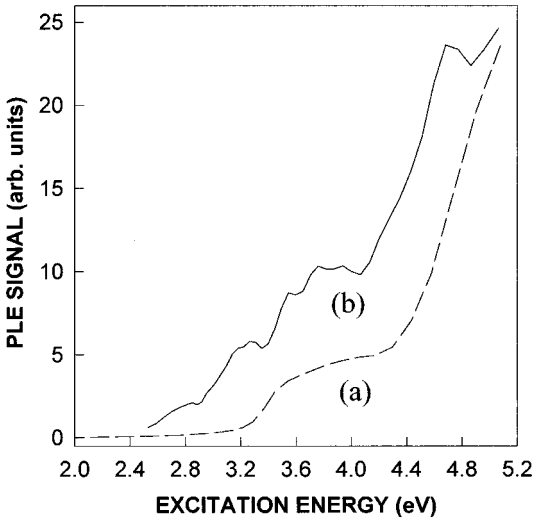

FIG. 8. Normalized PLE spectrum of a sample of oxygen passivated nc-Si with average Si cores of 2 nm [curve (b)], and the normalized absorption coefficient derived from Maxwell-Garnett formula using bulk Si dielectric function for a system of Si dots of average diameters of 2 nm [curve (a)].

and PL broadening with reduction of nanocrystal size can also be explained by a model involving absorption in the quantum confined Si cores, and emission due to transitions between dangling bond or defect states in the passivation layers. This latter point will be discussed in more detail in the next section.

PL decay times for passivated nc-Si varied from sample to sample, but were observed to increase for lower emission energies, as reported for porous Si by some other workers.[31,32] In Fig. 7, the top curve represents a PL decay time, faster than the laser pulse (20 ns), from the oxygen passivated nc-Si sample with orange-white PL (bottom curve in Fig. 5). The middle curve represents a single exponential PL decay with a time constant of about 70 ns from the oxygen passivated nc-Si sample with bright red PL (middle curve in Fig. 5). The bottom curve represents a single exponential PL decay with a time constant of 2μs from the hydrogen passivated nc-Si sample with infrared PL (topmost curve in Fig. 4). Here, we observed some similarities between PL decay times of our passivated nc-Si and porous Si. Porous Si with red emission usually has PL decay times on the order of microseconds, while green or blue PL from oxidized porous Si usually has decay times on the order of nanoseconds or less.[11,32–34]

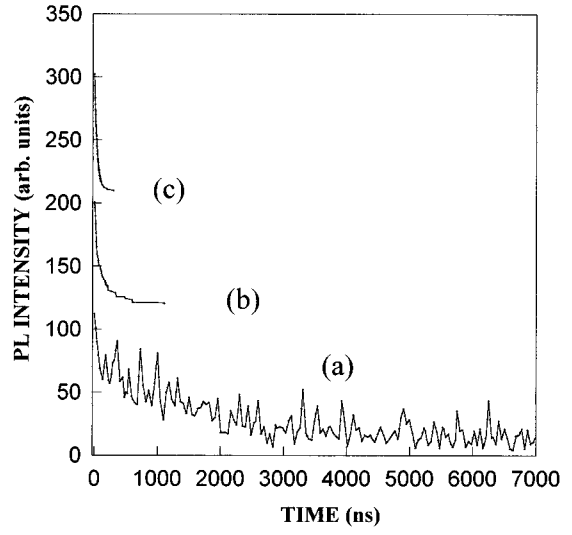

FIG. 7. PL decay times from (a) oxygen passivated nc-Si with orange-white PL, (b) oxygen passivated nc-Si with bright red PL, and (c) hydrogen passivated nc-Si with infrared PL.

In Fig. 8, we show the PLE spectrum from a 50-nm-thick sample of oxygen passivated nc-Si [curve (b)]. This was the same sample that yielded the PL in curve (a) of Fig. 5. For a film much thinner than the attenuation length of the exciting light, PLE data are proportional to the absorption coefficient of the film.[35] In fact, this PLE data curve qualitatively resembles the absorption coefficient [curve (a), offset by an arbitrary multiplicative factor] calculated from the Maxwell-Garnett formula[36] using the dielectric function of bulk Si. This formula, which allows the calculation of the effective absorption coefficient of a composite medium consisting of Si dots embedded in an SiO_2 matrix, is written as

$$\frac{\epsilon_{\text{eff}}(\omega)-1}{\epsilon_{\text{eff}}(\omega)+2}=p\frac{\epsilon(\omega)-1}{\epsilon(\omega)+2}. \tag{1}$$

Here p is the average volume fraction occupied by the Si dots. $\epsilon(\omega)$ is the complex frequency-dependent ratio of the dielectric function of bulk Si to the dielectric function of SiO_2. And $\epsilon_{\text{eff}}(\omega)$ is the complex effective dielectric function of the composite medium. The frequency-dependent absorption coefficient $\alpha(\omega)$ of the composite medium is given by

$$\alpha(\omega)\propto\omega\ \text{Im}[\epsilon_{\text{eff}}(\omega)], \tag{2}$$

where $\text{Im}[\epsilon_{\text{eff}}(\omega)]$ is the imaginary part of the complex effective dielectric function of the composite medium. This Maxwell-Garnett effective absorption coefficient curve was

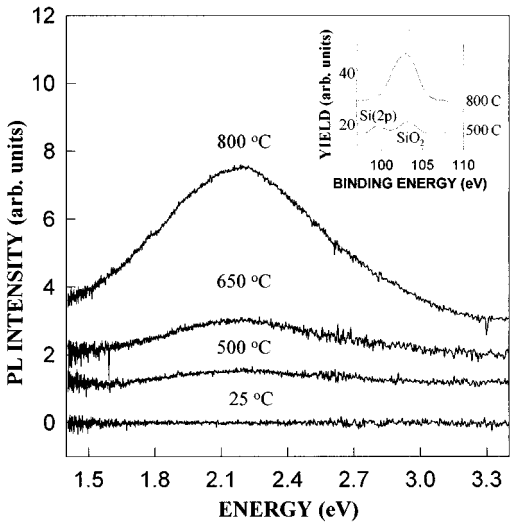

FIG. 9. PL intensities of a sample of oxygen passivated nc-Si as a function of annealing temperatures from 25 to 800 °C. The inset shows XPS signals from the same sample.

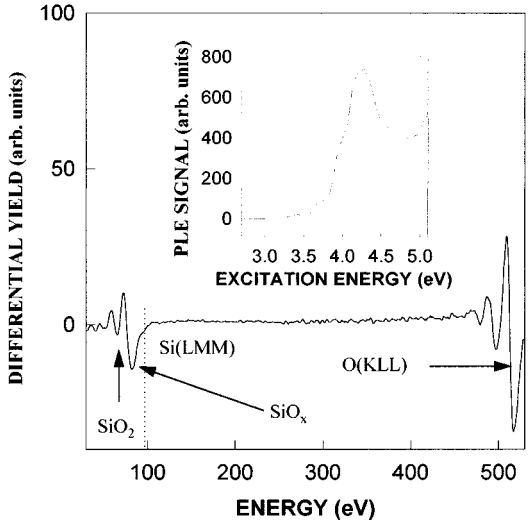

FIG. 10. Typical AES spectrum for an-SiO_x synthesized by vaporization of Si in an O_2 buffer gas. The inset shows the normalized PLE spectrum of the same sample.

derived from Eqs. (1) and (2), for a system of Si dots with average diameter of 2 nm and a size distribution as in curve (b) of Fig. 1, embedded in a SiO_2 matrix. Although the use of the bulk Si value for $\epsilon(\omega)$ does not account for the effects of band-structure changes due to quantum confinement in the nc-Si, it is certainly suitable for a rough comparison with the PLE spectra. Note that since both curves in Fig. 8 have been normalized by arbitrary multiplicative factors, only the shapes of these curves can be compared, not their absolute values. In general, the PLE data and the calculated absorption coefficient have similar shapes. A steep rise in the absorption starting above 4.1 eV, and an absorption plateau between 3.5 and 4.1 eV are observed in both the PLE and Maxwell-Garnett curves. However, in the energy range below the bulk direct interband transition of about 3.2 eV, the experimental PLE curve has a magnitude that is much greater than the calculated curve. This difference may be due to defect absorption in the SiO_x $(0<x\leqslant 2)$ layers covering the Si dots, which was, of course, not included in the Maxwell-Garnett calculation. The experimental PLE curve also has structures that are not found on the calculated curve. These structures are real and reproducible. They could be due either to absorption from various defects in the SiO_x $(0<x\leqslant 2)$ layers covering the nc-Si or to the quantization of electronic density of states of small dots, or both. It is most likely, however, that these structures result from defect absorption in SiO_x, since they are also seen in the energy range below 3.2 eV, where the absorption coefficient of bulk Si is very small. It is concluded from the above discussion that, apart from a small contribution from defect absorption, strong absorption in the quantum confined Si cores of the passivated nc-Si creates the excitations responsible for the PL.

For all samples of oxygen passivated nc-Si, the PL intensities increased after annealing in dry oxygen at 4×10^{-4} Torr up to 800 °C, without any accompanying PL peak shift. But a slight reduction in PL intensity was observed after postannealing to 900 °C. Figure 9 shows the effect of annealing at up to 800 °C in dry O_2 on PL intensity of the same sample as in curve *a* of Fig. 5. Similar behavior has also been observed for porous Si and Si ultrafine particles.[37–39] The inset of Fig. 9 shows XPS data from the same sample as a function of annealing in oxygen. The peak near 99.5 eV binding energy is due to photoelectrons from the Si $2p$ core-level transition in bulk crystalline Si. This peak shifts to about 103.5 eV for SiO_2. Smaller shifts are expected for intermediate oxidation states of Si in SiO_x $(0<x<2)$. These data show that the ratios of SiO_x to Si $(0<x\leqslant 2)$ increase as a function of annealing temperature from 500 °C to 800 °C. Note that the absence of a peak near 99.5 eV in the upper XPS curve in the inset does not imply that the nc-Si crystallites have been completely oxidized, because XPS is a surface sensitive technique and a signal from a silicon core may be unobservable.[40,41] Moreover, HRTEM and PLE measurements on the same sample have shown the existence of unoxidized Si cores after oxidation [curve (b), Fig. 1, and Fig. 8]. Our speculation is that the thickness of the Si oxide outer layer has been established by the low-temperature annealing. Nevertheless, this SiO_x layer had a significant amount of Si and oxygen dangling bonds, thus a nonstoichiometric Si/O ratio. Short annealing at higher temperatures simply passivated the dangling bonds more effectively, therefore achieving a more stoichiometric Si/O ratio (with x increased toward 2), leading to improved PL intensity without any accompanying PL peak shift. Nonetheless, a reduction in PL intensity at an annealing temperature of about 900 °C is not a complete surprise. The native oxide layer grown on a Si wafer by air exposure is known to begin to vaporize at temperatures $\geqslant$850 °C;[42] so when the rate of Si suboxide vaporization is comparable to the corresponding rate of formation, dangling bonds could be produced at the Si-SiO_x interface of the nc-Si, and a reduction in PL intensity would be not be unexpected.

B. an-SiO_x

Figure 10 shows a typical AES spectrum for a sample of

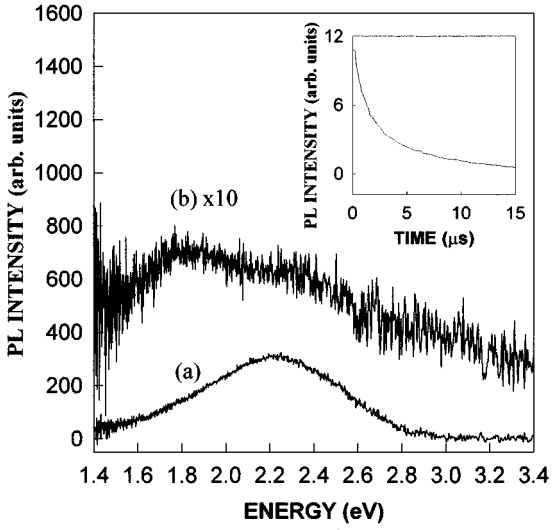

FIG. 11. PL spectra of an-SiO_x synthesized by vaporization of Si (a) at 1600 °C in and O_2 buffer gas of 3.5 mTorr and a source-to-substrate distance of 8 cm, and (b) by vaporization of Si at 1600 °C in an O_2 buffer gas of 2 mTorr and a source-to-substrate distance of 7 cm. The inset shows PL decay time of sample (a).

an-SiO_x synthesized by vaporization of Si in an O_2 buffer gas. The composition of the an-SiO_x was mostly SiO_x $(0<x\leqslant 2)$, since there was almost no signal from the Si (LMM) Auger transition in the AES spectrum at 92 eV. The O (KLL) Auger transition was observed at 503 eV. Note that no contamination was observed from the carbon boat or the tungsten basket. HRTEM revealed that these an-SiO_x films were networks of interlinking amorphous Si oxide nanostructures with occasional embedded Si dots with diameters less than 1 nm.

The inset of Fig. 10 shows a PLE spectrum of the same sample that yielded the AES curve in Fig. 10. This sample of an-SiO_x was deposited on HOPG by vaporization of Si at 1600 °C, in an O_2 buffer gas of 3.5 mTorr, and at a source-to-substrate distance of 8 cm. This PLE spectrum curve does not resemble that due to Si absorption (compare with Fig. 8). Therefore, the contribution of the occasionally embedded small Si dots to the net absorption is negligible. The excitation spectrum of an-SiO_x in Fig. 10 is similar to absorption spectra observed in nonstoichiometric SiO_x. For example, a strong absorption peak at about 4.2–4.3 eV was observed and identified with a type of oxygen deficiency defect center in silica.[43–46] The strong absorption in the energy range >5 eV in the PLE spectrum in Fig. 10 has also been reported for certain types of oxygen related defect centers in silica.[43,44]

Figure 11 shows PL spectra for two samples of an-SiO_x. Curve (a) was from the same sample that yielded the PLE spectrum in Fig. 10. This sample exhibited a strong and very broad orange-white PL, peaked at about 2.2 eV, with a biexponential PL decay with time constants of 1.2 and 7.8 μs (inset of Fig. 11). Note that the emission energies in this sample were much smaller than the absorption threshold energy. This indicates the existence of optical emission between trap states or lower-energy defect levels, which have absorption efficiencies several orders of magnitude smaller than the 4.3-eV absorption band.[43,45,46] The emission process is usually sensitive to such trapping states.[46] Also, broad PL peaks at about 1.9 and 2.3 eV were observed for oxygen related defect centers in amorphous Si oxide.[45] The PL decay of these centers was nonexponential with decay times from hundreds of nanoseconds to many tens of microseconds. The observed broad PL in curve (a) may originate from a combination of these two defect centers. Curve (b) was from a sample of an-SiO_x deposited on a Si wafer, which had been covered with a native oxide layer due to long exposure to ambient atmosphere. This sample was prepared by vaporization of Si at 1600 °C, in an O_2 buffer gas pressure of 2 mTorr, and at a source-to-substrate distance of 7 cm. There are several PL peaks recorded at around 1.7–1.9, 2.2–2.5, and 2.6–3.1 eV. All these PL bands have been reported for different types of oxygen-related defects in Si oxide.[7,45,47] We conclude that the emission and absorption from an-SiO_x are dominated by defect centers in the oxide.

Similar to the case of oxygen passivated nc-Si, the PL intensities of these two an-SiO_x samples increased with annealing in dry oxygen at 4×10^{-4} Torr up to 800 °C without any PL peak shift. So, even though all an-SiO_x samples were composed mostly of SiO_x $(0<x\leqslant 2)$, they shared many common PL properties with oxygen passivated nc-Si: very broad PL, many PL peaks in similar energy regions, and increasing PL intensities without PL peak shift after annealing in dry oxygen.

IV. DISCUSSION AND CONCLUSION

The experiments presented in this paper show that, for passivated nc-Si, absorption occurs between the quantum confined electronic states of the Si cores. PL blueshifts occur as the size of nc-Si crystallites is reduced. These observations clearly indicate the importance of the quantum confinement effect on the optical absorption properties of nc-Si. As far as the PL mechanism is concerned, it seems that a simple band-to-band recombination mechanism within the Si cores cannot be ruled out. There are, however, some properties of the PL that suggest a different explanation: (1) the differences in PL spectra for hydrogen passivated nc-Si and oxygen passivated nc-Si and (2) the PL properties of the oxygen passivated nc-Si have some similarities to those of the an-SiO_x samples, for which oxide defect states apparently play a dominant role in the PL. These properties lead us to believe that defect centers, rather than band-to-band recombination in the Si nanocrystals, are more likely to be responsible for the PL of the nc-Si films.

For many nanocrystals of comparable sizes, hydrogen passivated nc-Si had PL spectra that were redshifted in comparison with the corresponding PL spectra from oxygen passivated nc-Si [Figs. 4(a) and 5(b)]. In addition, the PL intensities from hydrogen passivated nc-Si films were usually weaker than those from oxygen passivated nc-Si films of comparable thicknesses. These effects may have been caused by imperfect passivation for our hydrogen passivated nc-Si, and they indicate a strong influence of surface and/or interface states in the recombination process of nc-Si.[9,11,12,17,31,32,48] The fact that PL decay times of our passivated nc-Si varied from sample to sample and increased with lower emission energies implies the coexistence of

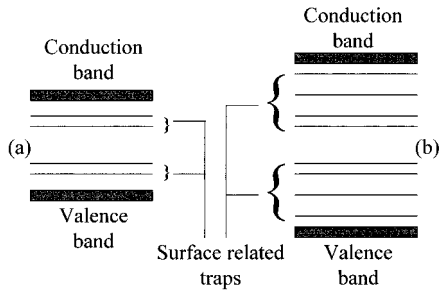

FIG. 12. Energy diagrams, including surface related traps, of (a) large quantum dots, and (b) small quantum dots.

competing radiative and nonradiative recombination processes. These competing processes may be related to surface conditions such as residual dangling bonds, surface stress and/or strain, and Si oxide defects at or near the surface.[11,12,31] In fact, the many common PL properties for oxygen passivated nc-Si and an-SiO_x, pointed out at the end of Sec. III, suggest that the radiative recombination processes in both materials are dominated by transition through defect centers. These defect centers are located in the oxide layer or at the boundary between this layer and the Si crystallite.[6,7,11] We conclude by discussing these properties with reference to this alternative model of the PL in nc-Si.

We propose that our data concerning passivated nc-Si can be best explained by a model involving absorption in the quantum confined Si cores and emission, which involves electronic transitions between surface and/or interface states.[6,9,11,12] This model can explain PL blueshifts with decreasing nanocrystal size, as well as the surface sensitive property of the PL from nc-Si. We now show how this model can explain qualitatively the PL blueshift with decreasing nanocrystal size, accompanied by PL broadening, observed in our PL data. Figure 12 is a diagram showing the energy levels near the surface of two sizes of Si quantum dots. It should be noted that these diagrams refer to ensembles of dots of a given size; the detailed energy levels for a particular size may vary from dot to dot depending on surface-interface configuration. In (a), the dots are bigger than the ones in (b), which have larger quantum confined energy gaps. Upon absorption of photons of proper energies, electrons and holes are generated in the conduction and valence bands of the dots. But due to the existence of surface related traps with energy levels extending into the energy gaps, there is a possibility of carriers getting trapped by, and subsequently recombined through, these gap states.[9,11,12,17,31,32,48] A PL blueshift with reducing nanocrystal size is possible, since carriers generated in the smaller dots may have access to gap states with trapping energies higher than the energy gap of the bigger dots. Broad PL spectra are also expected. On the basis of the diagram in Fig. 12, it might be expected, indeed, that the PL bandwidth will increase with increasing energy gap. This is because carriers generated in the smaller dots may also have access to gap states with much smaller trapping energies. So, depending on the relative densities and recombination efficiencies of the different surface states involved, a PL broadening may accompany the PL blueshift of the small dots. This has been observed in our data in Fig. 5, where the bandwidth in curve (a) is substantially larger than the visible counterpart in (b). The different properties of oxygen and hydrogen passivated dots reflect the differences in the energy distribution, lifetimes, and other properties of the surface or interface states. In particular, the longer wavelength emission in hydrogen passivated dots is caused by a prevalence of surface states lying deeper in the energy gap than for oxygen passivated dots.

In conclusion, we have synthesized nc-Si, the size of which can be controlled. When passivated by hydrogen or oxygen, these nc-Si showed strong infrared and/or visible PL. The PL properties of these nc-Si can be best explained by a model involving absorption in the quantum confined Si cores and emission due to transition between defect states in the passivation layer. However, a simple band-to-band recombination mechanism within the Si cores cannot be completely ruled out.

ACKNOWLEDGMENTS

We thank Dr. Margaret Olsen for her HRTEM measurements and to Dr. A. V. Hamza, Dr. Tony Van Buuren, and Dr. L. J. Terminello for helpful discussions. This work was supported by the Division of Materials Sciences, Office of Basic Energy Science, U.S. Department of Energy, and performed under the auspices of the U.S. Department of Energy by Lawrence Livermore National Laboratory under Contract No. W-7405-ENG-48.

[1] L. T. Canham, Appl. Phys. Lett. **57**, 1046 (1990).
[2] H. Takagi, H. Ogawa, Y. Yamazaki, A. Ishizaki, and T. Nakagiri, Appl. Phys. Lett. **56**, 379 (1990).
[3] H. Morisaki, H. Hashimoto, F. W. Ping, H. Nozawa, and H. Ono, Appl. Phys. Lett. **27**, 2977 (1933).
[4] Qi Zhang, S. C. Bayliss, and D. A. Hutt, Appl. Phys. Lett. **66**, 1977 (1995).
[5] S. M. Prokes, and O. J. Glembocki, Mater. Chem. Phys. **35**, 1 (1993).
[6] Y. Kanemitsu, T. Ogawa, K. Shiraishi, and K. Takeda, Phys. Rev. B **48**, 4883 (1993).
[7] S. M. Prokes and W. E. Carlos, Appl. Phys. Lett. **78**, 2671 (1995).
[8] S. Schuppler, S. L. Friedman, M. A. Marcus, D. L. Adler, Y. H. Xie, F. M. Ross, Y. J. Chabal, T. D. Harris, L. E. Brus, W. L. Brown, E. E. Chaban, P. F. Szajowski, S. B. Christman, and P. H. Citrin, Phys. Rev. B **52**, 4910 (1995).
[9] F. Koch, V. Petrova-Koch, and T. Muschik, J. Lumin. **57**, 271 (1993).
[10] J. S. Tse, J. R. Dahn, and F. Buda, J. Phys. Chem. **99**, 1896 (1995).
[11] L. Tsybeskov, J. V. Vandyshev, and P. M. Fauchet, Phys. Rev. B **49**, 7821 (1994).
[12] M. Yamada, A. Takazawa, and T. Tamura, Jpn. J. Appl. Phys. **31**, L1451 (1992).
[13] W. L. Wilson, P. F. Szajowski, and L. E. Brus, Science **262**, 1242 (1993).

[14] R. P. Vasquez, R. W. Fathauer, T. George, A. Ksendzow, and T. L. Lin, Appl. Phys. Lett. **60**, 1004 (1992).
[15] T. Goerge, M. S. Anderson, W. T. Pike, T. L. Lin, R. W. Fathauer, K. H. Jung, and D. L. Wong, Appl. Phys. Lett. **60**, 2359 (1992).
[16] M. S. Brandt, H. D. Fuchs, M. Stutzmann, J. Weber, and M. Cardona, Solid State Commun. **81**, 302 (1992).
[17] S. M. Prokes, O. J. Glembocki, V. M. Bermudez, R. Kaplan, L. E. Friedersdorf, and P. C. Searson, Phys. Rev. B **45**, 13 788 (1992).
[18] K. H. Li, C. Tsai, J. Sarathy, and J. C. Campbell, Appl. Phys. Lett. **62**, 3192 (1993).
[19] S. M. Prokes and O. J. Glembocki, Phys. Rev. B **49**, 2238 (1994).
[20] S. Yatsuya, S. Kasukabe, and R. Uyeda, J. Cryst. Growth **24/25**, 319 (1974).
[21] S. Hayashi, S. Tanimoto, and K. Yamamoto, J. Appl. Phys. **68**, 5300 (1990).
[22] J. J. Boland, J. Vac. Sci. Technol. A **10**, 2458 (1992).
[23] J. W. Lyding, G. C. Abelin, T. C. Shen, C. Wang, and J. R. Tucker, J. Vac. Sci. Technol. B **12**, 3735 (1994).
[24] Due to convolution of the cluster dimensions with the finite radius of the STM tip, STM diameter measurements tended to give values that could be up to 20% higher than the actual values (i.e., those determined from HRTEM and XRD). On the other hand, STM height measurements of nc-Si on HOPG yielded values that could be up to 200% lower than actual values. This is because near the Fermi level, where most electrons of the tunneling current come from, a semimetal such as graphite usually has a much higher electronic density of states than that of a semiconductor such as Si. This causes the tip to approach much closer to the Si nanocrystal than to the graphite substrate for a given tunneling current, and the height of the nanocrystal is therefore underestimated by STM. Height measurements where therefore not used to determine nanocrystal sizes.
[25] B. D. Cullity, *X-ray Diffraction* (Addison-Wesley, Reading, MA, 1956).
[26] V. Lehmann, B. Jobst, T. Muschik, A. Kux, and V. Petrova-Koch, Jpn. J. Appl. Phys. **32**, 2095 (1993).
[27] V. Petrova-Koch and T. Muschik, Thin Solid Films **255**, 246 (1995).
[28] Y. Mochizuki, M. Mizuta, Y. Ochiai, S. Matsui, and N. Ohkubo, Phys. Rev. B. **46**, 12 353 (1992).
[29] N. A. Hill and K. B. Whaley, Phys. Rev. Lett. **75**, 1130 (1995).
[30] L. W. Wang and A. Zunger, J. Phys. Chem. **98**, 2158 (1994).
[31] T. Miyoshi, K. S. Lee, and Y. Aoyagi, Jpn. J. Appl. Phys. **31**, 2470 (1992).
[32] L. R. Tessler, F. Alvarez, and O. Teschke, Appl. Phys. Lett. **62**, 2381 (1993).
[33] Y. Kanemitsu, T. Futagi, T. Matsumoto, and H. Mimura, Phys. Rev. B **49**, 14 732 (1994).
[34] C. Delerue, M. Lannoo, and G. Allan, J. Lumin. **57**, 249 (1993).
[35] L. Wang, M. T. Wilson, and N. M. Haegel, Appl. Phys. Lett. **62**, 1113 (1993).
[36] L. Banyai and S. W. Koch, *Semiconductor Quantum Dots* (World Scientific, Singapore, 1993), Chap. 2.
[37] S. M. Prokes, Appl. Phys. Lett. **62**, 3244 (1993).
[38] P. Wickboldt, H. M. Cheong, D. Pang, J. H. Chen, and W. Paul, in *Microcrystalline and Nanocrystalline Semiconductors*, edited by L. Brus *et al.*, MRS Symposia Proceedings No. 358 (Materials Research Society, Pittsburgh, 1995), p. 127
[39] A. J. Kontkiewicz, A. M. Kontkiewicz, J. Siejka, S. Sen, G. Nowak, A. M. Hoff, P. Sakthivel, K. Ahmed, P. Mukherjee, S. Witanachchi, and J. Lagowksi, Appl. Phys. Lett. **65**, 1436 (1994).
[40] C. D. Wagner, W. M. Riggs, L. E. Davis, J. F. Moulder, and G. E. Muilenberg, *Handbook of X-Ray Photoelectron Spectroscopy* (Perkin-Elmer Corp., Eden Prairie, MN, 1979).
[41] L. N. Dinh, L. L. Chase, M. Balooch, L. J. Terminello, and F. Wooten, Appl. Phys. Lett. **65**, 3111 (1994).
[42] L. N. Dinh, M. Balooch, and L. L. Chase (unpublished).
[43] H. Nishikawa, T. Shiroyama, R. Nakamura, Y. Ohki, K. Nagasawa, and Y. Hama, Phys. Rev. B **45**, 586 (1992).
[44] L. N. Skuja, A. N. Streletsky, and A. B. Pakovich, Solid State Commun. **50**, 1069 (1984).
[45] J. H. Stathis and M. A. Kastner, Phys. Rev. B **35**, 2972 (1987).
[46] A. Kux, D. Kovalev, and F. Koch, Thin Solid Films **255**, 143 (1995).
[47] I. A. Movtchan, R. W. Dreyfus, W. Marine, M. Sentis, M. Autric, G. Lelay, N. Merk, This Solid Films **255**, 286 (1995).
[48] L. Tsybeskov and P. M. Fauchet, Appl. Phys. Lett. **64**, 1983 (1994).